Biosensors and Bioelectronics 127 (2019) 155–160

Contents lists available at ScienceDirect

Biosensors and Bioelectronics

journal homepage: www.elsevier.com/locate/bios

An electrochemical DNA biosensor analytic technique for identifying DNA methylation specific sites and quantify DNA methylation level

Jian Huang[a,b,1], Shu Zhang[c,d,1], Fei Mo[c,d], Shasha Su[d], Xi Chen[d], Yan Li[a], Lichao Fang[a], Hui Huang[a], Jun Deng[a], Huamin Liu[a], Xiaoli Yang[e,*], Junsong Zheng[a,*]

[a] Department of Clinical and military Laboratory Medicine, Army Medical University, 30 Gaotanyan Street, Shapingba District, Chongqing 400038, China
[b] Department of Clinical Biochemistry, Affiliated Hospital of Guizhou Medical University, Guiyang 550004, China
[c] Department of Clinical Laboratory, Affiliated Hospital of Guizhou Medical University, Guiyang 550004, China
[d] Medical Laboratory, Guizhou Medical University, Guiyang 550525, China
[e] Department of laboratory medicine, the General Hospital of Chinese People's Armed Police Forces, Beijing 100039, China

ARTICLE INFO

Keywords:
Electrochemical biosensor
DNA methylation
Hydrophobic sphere
Steric hindrance

ABSTRACT

We herein developed a novel electrochemical biosensor to detect DNA methylation level, and to quantitatively analyze multiple methylated sites. Graphene oxide was modified with anti-5-methylcytosine antibody to specifically bind CpG methylation sites, and horseradish peroxidase (HRP)-labeled IgG secondary antibody was bound to the former antibody. In buffer containing H_2O_2 and hydroquinone, HRP-IgG catalyzed the oxidation of hydroquinone into benzoquinone over H_2O_2, thereby generating electrochemical reduction signals. The number of 5-methylcytosine was directly proportional to current signal, thereby allowing accurate quantification of methylation level. We also analyzed monomethylated target sequences with different sites. After different methylated sites were captured by the probe, the steric hindrance differences between $-CH_3$ hydrophobic sphere and the electrode surface were induced. The peak current decreased with reducing distance from the electrode surface, so DNA methylation sites were identified by measuring corresponding peak current responses. With a low detection limit (1 fM), this DNA biosensor was suitable for ultrasensitive DNA methylation detection. The linear detection range was 10^{-15} M to 10^{-8} M. Meanwhile, this method had high specificity, stability and repeatability, thus being widely applicable to the clinical detection of DNA methylation.

1. Introduction

DNA methylation, as one of the most extensively studied epigenetic modifications, plays an important role in the regulation of gene expression during development (Smith and Meissner, 2013). DNA methylation regulates gene expression by recruiting proteins involved in gene suppression or by preventing transcription factors from binding DNA. Its main functions include regulation of expressions of tissue-specific genes, silencing of reverse transcription elements, gene imprinting and X chromosome inactivation (Moore et al., 2012). At present, DNA methylation detection has become a new strategy for the early warning of tumors and the clinical diagnosis of epigenetic and genetic disorders (Assenov et al., 2014; Kader and Ghai, 2015; Schubeler, 2015; Stefansson et al., 2015; Visvanathan et al., 2016). Many researchers have identified the methylations of genes such as lung cancer *death-associated protein kinase 1*, *Ras association domain family 1 A,* liver cancer circulating tumor DNA, colon cancer *cyclin-dependent kinase inhibitor 2 A* and leukemia *P15 INK4B* as the early markers of tumorigenesis. Therefore, accurately localizing methylation in different regions of specific genes and determining their methylation levels are of great significance to the early prevention and treatment of tumors (Agrawal et al., 2007; Coppedè, 2014; Andresen et al., 2015; Bock et al., 2016; Jones et al., 2016; Stieglitz et al., 2017; Xu et al., 2017).

Up to now, a variety of DNA methylation detection strategies have been proposed, which are roughly classified into three types: methylation-sensitive restriction endonuclease (MSRE) analysis, Bisulfite-Seq analysis and quantification of DNA methylation levels based on methyltransferase activity measurement (Flusberg et al., 2010; Laird, 2010; Bakshi et al., 2015; Ziller et al., 2015). However, these methods still have some limitations. Although Bisulfite-Seq analysis is currently the sole available method for analyzing methylated sites and measuring

* Corresponding authors.
E-mail addresses: yangxiaolitwins@163.com (X. Yang), zhengalpha@sina.com (J. Zheng).
[1] The two authors contributed equally to this study.

https://doi.org/10.1016/j.bios.2018.12.022
Received 26 August 2018; Received in revised form 7 December 2018; Accepted 10 December 2018
Available online 16 December 2018
0956-5663/

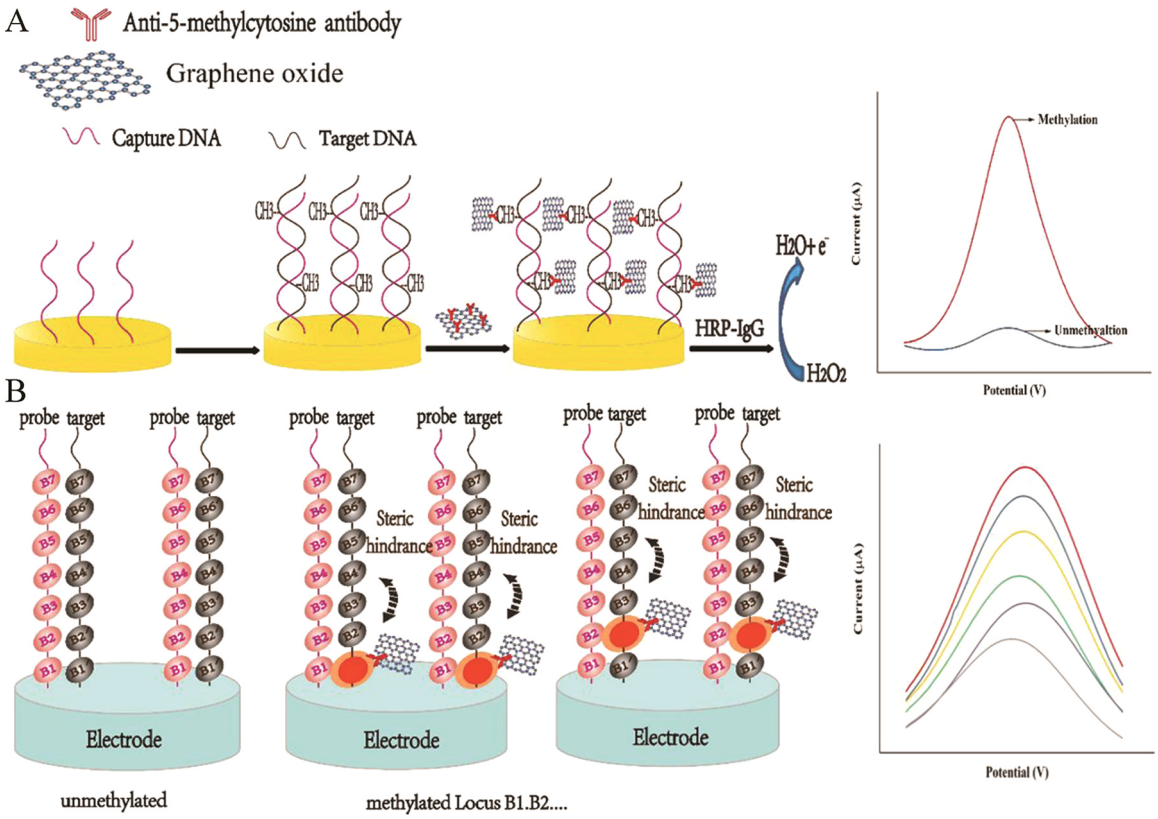

Fig. 1. Schematic representation of the developed method for DNA methylation detection. A: Schematic diagram of the electrochemical detection system; B: mechanism for analysis of DNA methylation sites by this biosensor. After binding of different methylated sites from the electrode surface to anti-5-methylcytosine antibody-modified GO, different DPV current signals are produced responding to steric hindrance differences.

methylation level, the entire process is complicated and time-consuming, also requiring expensive apparatus and complex data analysis. Due to the recognition specificity of base sequences by restriction endonuclease (RE), MSRE analysis has a limited detection range. More importantly, this technique cannot determine the levels or exact sites of methylation (Schalkwyk et al., 2010; Cheow et al., 2015; Guo et al., 2017; Mulqueen et al., 2018). By measuring methyltransferase activity, this method only indirectly reflects DNA methylation level, so it may not be most reliable because of internal environment differences (Flusberg et al., 2010; Laird, 2010; Bakshi et al., 2015; Yu et al., 2018). In contrast, electrochemical biosensing has attracted wide attention owing to facile operation, high sensitivity and selectivity, as well as easy miniaturization (Hansen et al., 2011; Muren and Barton, 2013; Ziller et al., 2015; Labib et al., 2016; Krejcova et al., 2017). Kato et al. proposed an electrochemical method to explore DNA methylation in CpG oligonucleotides that were directly oxidized by a nanocarbon film electrode (Kato et al., 2011). Besides, Wang et al. employed a methyltransferase-restriction endonuclease technique to detect the activity of DNA methyltransferase using anti-5-methylcytosine antibody and horseradish peroxidase (HRP)-labeled IgG (Wang et al., 2012). Using DNA-AuNPs as a signal amplification unit, Jing et al. analyzed DNA methylation and methyltransferase activity by detecting the electrochemical signals of methylene blue in residual nucleic acid chains on the Au electrode surface (Jing et al., 2014). Although each method has its merits, they all fail to accurately quantify DNA methylation levels or to localize the methylated sites.

In this study, we proposed a highly sensitive and selective method to detect DNA methylation based on the transduction of signals induced by steric hindrance on the nanoscale. Increase of methyl group on the DNA molecule surface is the sole structural change after methylation. In the liquid phase, methylated DNA forms a hydrophobic sphere with methyl group as the core on the surface of methylated cytosine, as a molecular characteristic for electrochemical sensing. Hydrophobic methyl sphere inevitably changes the spatial distribution of conducting medium in the microenvironment of electrode surface film for methylated DNA with 5-methylcytosine as the center. After different methylated sites bind a capture probe, steric hindrance differences are induced from the hydrophobic sphere to the electrode surface. As a result, steric hindrance and occupation of the reaction medium on the electrode surface are changed, further varying electrochemical response signals such as electrical impedance and peak current (Tian et al., 2014; Mahshid et al., 2015, 2017). In this way, differences between the methylated sites of DNA sequence are converted into electrochemical response signals for localization and analysis. Furthermore, DNA methylation level (amount of 5-methylcytosine) can be quantified.

As a novel carbon material, graphene oxide (GO) has large specific surface area and considerable functional groups (e.g. hydroxyl and carboxyl) on the surface, thus allowing biological conjugation and extensive applications to electrochemical biosensing. On the basis of GO and RE, Li et al. specifically detected DNA methylation and methyltransferase activity (Li et al., 2012). They augmented the detection sensitivity through GO signal amplification, i.e. GO-amplified electrogenerated chemiluminescence. Additionally, Yang et al. developed an ultrasensitive electrochemical immunosensor for prostate cancer based on a GO/thionine composite that immobilized high proportions of HRP and signal antibody through glutaraldehyde cross-linking for signal tracing (Yang et al., 2010). They improved the detection of prostate-specific antigen by elevating the enzyme immobilization amount and synergizing with enzymatic catalysis. Likewise, researchers have endeavored to functionalize GO by using various methods to immobilize antibodies for ultrasensitive electrochemical immunosensing (Wan et al., 2011; Haque et al., 2012; Lin et al., 2012; Saleem et al., 2016). Anti-5-methylcytosine antibody has been reported to specifically recognize methylated cytosines in single- and double-stranded DNAs

(Wang et al., 2012; Yang et al., 2015; Gao et al., 2017). Thereby motivated, we herein modified GO with anti-5-methylcytosine antibody to detect DNA methylation level and to localize methylated sites. The GO surface was rich in carboxyl groups that adsorbed considerable antibodies, thus substantially augmented the detection sensitivity and signal (Deng et al., 2016; Natarajan et al., 2017). As shown in Fig. 1, anti-5-methylcytosine antibody-modified GO is specifically bound to CpG methylation sites. Then rabbit anti-mouse HRP-IgG secondary antibody further specifically bound anti-5-methylcytosine antibody. HRP catalyzed the oxidation of hydroquinone into benzoquinone over H_2O_2, generating oxidation current that was converted into detectable electrochemical signal. The number of 5-methylcytosine was directly proportional to current signal, thereby allowing accurate quantification of methylation level. Also, we analyzed monomethylated target sequences with different sites. After being captured by the DNA probe, various methylated sites were identified by measuring peak currents in response to the steric hindrance differences between -CH_3 hydrophobic sphere and the electrode surface.

2. Materials and methods

2.1. Reagents and materials

The reagents and materials used in this study are presented in Supporting information.

2.2. Apparatus

The apparatus used in this study is presented in Supporting Information.

2.3. Preparation of anti-5-methylcytosine antibody-modified GO

According to a previous study (Xu et al., 2015), GO (10 mg) was first diluted with ultrapure water to 2 mg/mL, and completely dispersed through ultrasonication in a water bath. Then pH of the solution was adjusted to 4.5 by adding diluted HCl solution. Afterwards, the GO concentration was adjusted to 5 mM by adding 2×10^{-3} mol/L sulfo-N-hydroxysuccinimide (NHS) and 8×10^{-3} mol/L N-(3-dimethylaminopropyl)-N'-ethylcarbodiimide hydrochloride, and the solution was dispersed for 30 min. The resulting GO solution was centrifuged, and the precipitate was washed twice to three times by using pH 4.5 HCl solution. The residue was resuspended by pH 8.0 PBS, followed by addition of 15 μL of anti-5-methylcytosine antibody (0.5 mg/mL) and storage in a 4 °C refrigerator overnight. The suspension was washed three times by centrifugation as mentioned above, and the supernatant was removed. Then the precipitate was resuspended by PBS to remove excess antibody and to release NHS. Finally, the residue was suspended again by 1 mL of PBS.

2.4. Preparation of AuNPs/Au electrode

Gold electrode was polished with 0.3 μm and 0.05 μm Al_2O_3 slurries until a mirror surface formed, and rinsed ultrasonically with ultrapure water, absolute ethanol and ultrapure water for 5 min successively. After drying at room temperature, freshly prepared piranha solution (98% H_2SO_4: 30% H_2O_2, 3:1) was dropwise added onto the surface of the gold electrode which was activated for 20 min and then thoroughly rinsed with ultrapure water. Afterwards, the gold electrode was subjected to cyclic voltammetry (CV) in 0.5 M H_2SO_4 solution from −0.3 V to −1.6 V with a scan rate of 100 mV/s until a stable and repeatable CV curve was obtained. After activation, the gold electrode was rinsed with ultrapure water and dried with nitrogen gas prior to use. Subsequently, the electrode was placed in 3 mM $HAuCl_4$ solution, onto which gold nanoparticles were deposited through potentiostatic electrolysis (potential: −0.2 V, time: 120 s). After thorough washing with triply distilled water, the obtained AuNPs/Au electrode was finally prepared for DNA probe fixing, and characterized with scanning electron microscopy (SEM) and atomic force microscopy.

2.5. DNA probe fixing and hybridization

Briefly, 10 μL of fixing buffer (10 mM Tris-HCl, 1 mM EDTA, 50 mM NaCl and 1.0 mM tris(2-carboxyethyl)phosphine hydrochloride, pH 7.0) containing 1.0×10^{-7} M DNA S1 probe was dropped onto the surface of AuNPs/Au electrode to react at 4 °C for 12 h. The electrode was thereafter rinsed with PBS to remove free DNA probe. To further block non-specific binding sites, 20 μL of 1 mM 6-mercapto-1-hexanol (MCH) solution was dropped onto the electrode surface that was blocked at room temperature for 1 h, giving an MCH/DNA S1/AuNPs/Au electrode. The electrode was rinsed with PBS, and the surface was blown dry with nitrogen. Hybridization buffers containing 10 μL of 1.0×10^{-7} M different target sequences were dropped onto the modified electrode surface, and incubated at 37 °C for 2 h.

2.6. Fixing of anti-5-methylcytosine antibody and HRP-IgG antibody

After hybridization, the electrodes were incubated with 5% bovine serum albumin solution for 30 min to prevent any possible non-specific binding. After washing 3 times with 0.1 M PBS (pH 7.0), 10 μL of anti-5-methylcytosine antibody (10 μg/mL) was dropped onto the electrode surface, incubated for 1 h, and rinsed with 0.1 M PBS. Subsequently, 10 μL of HRP-IgG antibody (80 μg/mL) was dropped onto the electrode surface, incubated at room temperature for 30 min, rinsed 3 times with 0.1 M PBS and dried at room temperature. The detection lasted for approximately 5 h in total.

2.7. Electrochemical determination

Differential pulse voltammetry (DPV) was conducted in 10 mL of 0.1 M PBS (pH 7.0) containing 1 mM H_2O_2 and 1 mM hydroquinone. DPV signals were measured by using parameters as follows: initial potential, −0.3 V; terminal potential, 0.1 V; potential step, 4 mV; pulse amplitude, 50 mV; pulse width, 0.05 s; sampling width, 0.0167 s; pulse period, 0.2 s; rest time, 2 s.

3. Results and discussion

3.1. Characterizations of GO and anti-5-methylcytosine antibody-modified GO

The functional groups of different compounds can be characterized by Fourier transform infrared (FTIR) spectrometer to determine the compound types and changes of functional groups during reactions. The FTIR spectrum of GO (Fig. S1, red line) shows a broad and strong peak at about 3410 cm^{-1}, which can be assigned to the vibration of -OH. The absorption peak at 1724 cm^{-1} corresponds to C=O from the carboxyl group, and that at 1620 cm^{-1} may represent the vibration of C=C. In addition, the peaks at 1400 and 1077 cm^{-1} correspond to the bending vibration of C-OH and the vibration of C-O respectively. The black line in Fig. S1 (Supporting information) presents the FTIR spectrum of antibody-modified GO. The new peaks at 1226 and 1175 cm^{-1} can be assigned to the stretching vibration of C-O-C in saturated ester and the wagging vibration of NH_2 in primary amide respectively. Given that the peak characterizing antibody conjugation mainly originates from the amide bond, the modification was successful (Jin et al., 2012; Gong et al., 2017).

3.2. Electrochemical characterizations of different modified electrodes

The morphology of AuNPs/Au electrode was observed by SEM (Fig. S2). To test the surface properties of modified electrode, each

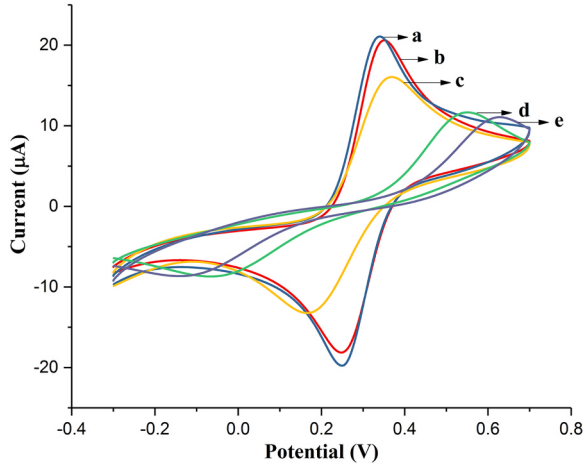

Fig. 2. CV curves obtained for different modified electrodes in 1 mM $[Fe(CN)_6]^{3-/4-}$ and 0.1 M KCl solution. (a) Bare gold electrode; (b) AuNPs/GE; (c) ssDNA/AuNPs/GE; (d) MCH/ssDNA/AuNPs/GE; (e) target DNA/MCH/ssDNA/AuNPs/GE.

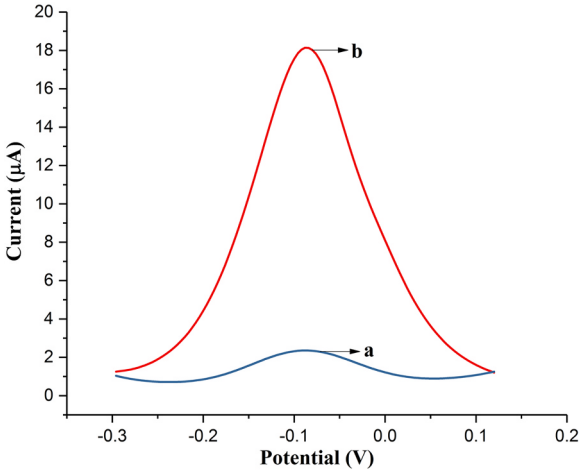

Fig. 3. DPV current signals in response to methylated (red) and unmethylated (blue) DNA sequences.

modification step of the working electrode was subjected to CV in PBS (pH 7.0) containing 1 mM $[Fe(CN)_6]^{3-/4-}$ and 0.1 M KCl. The CV curve of bare gold electrode shows a pair of distinct redox peaks (Fig. 2, curve a), indicating that the electron transfer of $[Fe(CN)_6]^{3-/4-}$ on the surface was very fast. After electrodeposition of gold nanoparticles, the redox peak current further increased because of enlarged effective surface area of the gold electrode and promoted electron transfer (curve b). When the capture probe was immobilized through the Au-S bond (curve c), its negative charge hindered the diffusion of electrons towards the gold electrode surface, thereby decreasing the redox peak current and enlarging the distance between two peaks. In short, the electrode surface had been successfully modified with this probe. MCH solution was used to further block non-specific binding sites on the gold electrode surface (curve d), which decreased the redox peak current and significantly increased the inter-peak distance by inhibiting redox diffusion. Hence, non-specific binding sites on the electrode surface were successfully blocked by MCH. After the capture probe hybridized with target sequences (curve e), the number of negative charges on the gold electrode surface continued to rise, so the electron transfer ability of $[Fe(CN)_6]^{3-/4-}$ was further attenuated, which then reduced the redox peak current. Collectively, each modification step of the electrochemical biosensor was successful. This was in accordance with the results of other studies (Jing et al., 2014; Gao. et al., 2017).

3.3. Validation of feasibility

The current response was weak without methylation (Fig. 3, curve a), because antibody that modified GO was non-specifically adsorbed onto double-stranded DNA. Curve b exhibits an obvious oxidation peak at −0.08 V after methylation, because double-stranded DNA contained methyl group that was specifically recognized by anti-5-methylcytosine antibody binding HRP-labeled secondary antibody. HRP catalyzed the oxidation of hydroquinone into benzoquinone over H_2O_2, generating oxidation current that was converted into detectable electrochemical signal (Wang et al., 2012). Taken together, this method was applicable to the detection of DNA methylation, following the process in Fig. 1.

3.4. Optimization of experimental conditions

To maximize the analysis performance, we then optimized the experimental conditions including hybridization time and antibody concentration (Fig. S3 and S4, Supporting information).

3.5. Quantification of DNA methylation levels

The current signal was directly related to the quantity of methylated cytosine. For the detection of DNA methylation levels, we prepared target sequences with known numbers of methylated sites (from 1 to 5). Fig. 4A shows that the DPV peak current is elevated with rising methylation level, and Fig. 4B indicates that the current is linearly related with the number of methylated sites. The correlation coefficient R was 0.9926, and the linear regression equation was I (μA) = 3.1455 + 6.6825 lg[C]. In a word, our method can be used to sensitively detect DNA methylation levels.

To evaluate the sensitivity of this biosensor, the DPV signal responses to different concentrations of target DNA sequence with only one methylated site under optimum conditions were recorded. As exhibited in Fig. 4C, the current increases with rising DNA concentration from 10^{-17} M to 10^{-6} M. Fig. 4D presents that the DPV peak current is well linearly related with the logarithm of target sequence concentration from 10^{-15} M to 10^{-8} M. The regression equation was I = 0.3173 Log C (M) + 6.4573, and the correlation coefficient R was 0.9903. Meanwhile, the limit of detection was 0.84 fM (based on 3σ/slope) (Kong et al., 2014). The comparisons of the proposed method with previous assays are listed in Table S2. As suggested by the linear range and detection limit, our method is superior to others (Kurita et al., 2012; Kong et al., 2014; Xu et al., 2014; Yao et al., 2014; Yin et al., 2014). Besides, most reported assays indirectly measured DNA methylation level by detecting the activity of methyltransferase, which may suffer from incomplete methylation (Zhang et al., 2015, 2017). Instead, our method can directly detect the number of DNA methylation sites.

3.6. Analysis of DNA methylation sites

According to previous literatures (Mahshid et al., 2015, 2017), the existence of macromolecules such as proteins was determined on the basis of steric hindrance. To accurately localize DNA methylation sites, we prepared target sequences with known ones (DNA S3, DNA S4, DNA S5, DNA S6 and DNA S7). As presented in Fig. 5, the methylated target sequence S3 closest to the electrode has the minimum DPV peak current which gradually rises with increasing distance of methylated site from the electrode surface. Probably, there was a steric hindrance difference

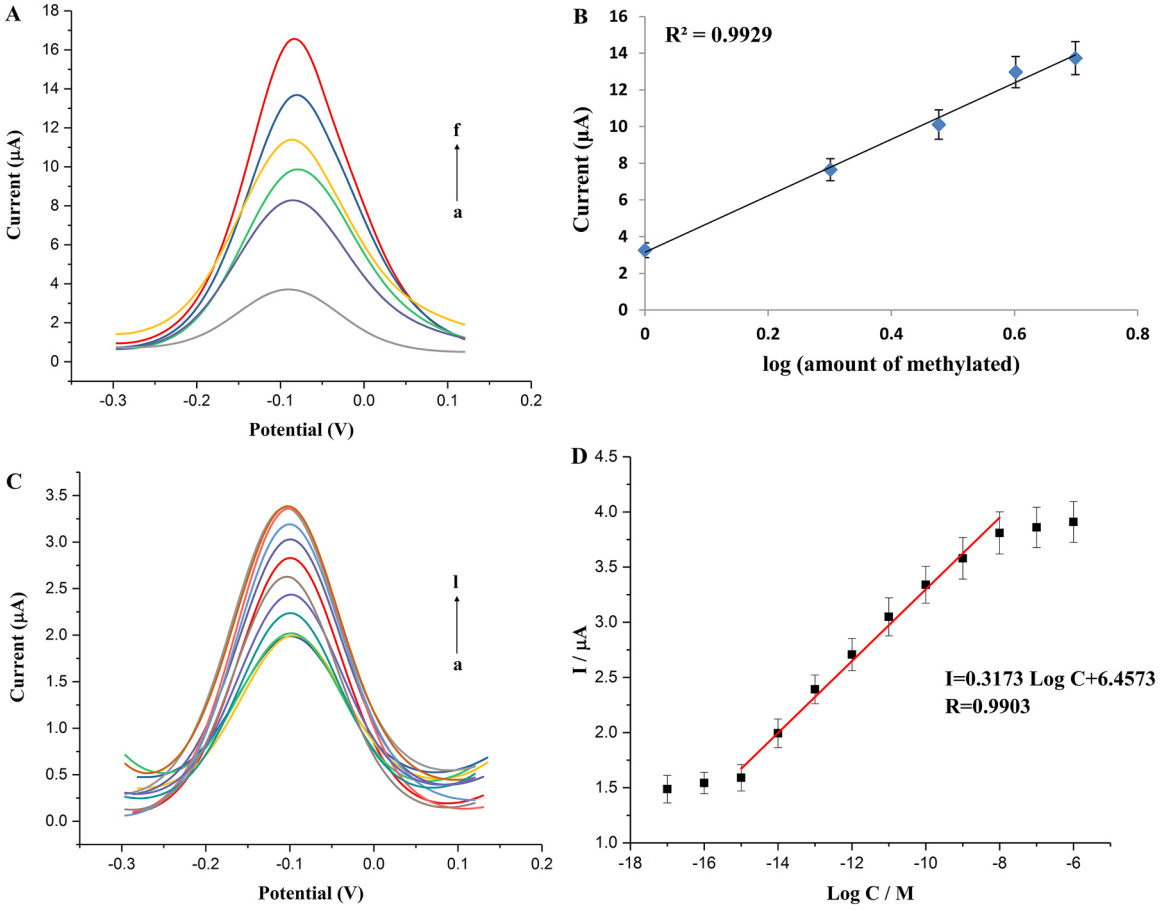

Fig. 4. (A) DPV results of sequences with different numbers of methylated and unmethylated sites. a-f: Without methylation, 1-site methylation, 2-site methylation, 3-site methylation, 4-site methylation and 5-site methylation, respectively. (B) Response voltammogram obtained with variable numbers of methylated sites from 1 to 5. (C) DPV responses of sequences with different concentrations of 1-site methylated DNA. a-l: 10^{-17} M, 10^{-16} M, 10^{-15} M, 10^{-14} M, 10^{-13} M, 10^{-12} M, 10^{-11} M, 10^{-10} M, 10^{-9} M, 10^{-8} M, 10^{-7} M and 10^{-6} M, respectively. (D) Linear relationship between peak current and logarithm of methylated DNA concentration.

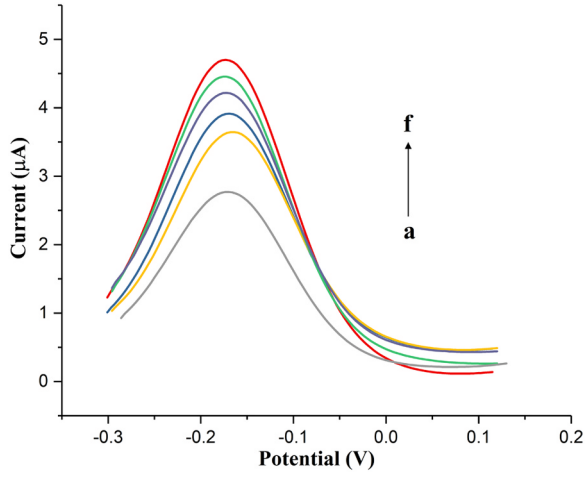

Fig. 5. DPV results of DNA methylation sites with different distances from electrode surface. a-f: DNAS2-DNAS7 respectively.

between hydrophobic methyl spheres and the electrode surface after different methylated sites bound the capture probe (Fig. 6). This difference was further augmented through binding with antibody-modified GO. Consequently, steric hindrance and occupation of the reaction medium on the electrode surface changed, ultimately generating different peak current signals.

3.7. Reproducibility and stability of sensor

We then tested the repeatability and stability of the proposed method by determining DNA sequence in which only one cytosine was methylated. Given that the relative standard deviation of six consecutive measurements of oxidation peak current of 5-methylcytosine was 6.49%, the repeatability of this method was acceptable. Moreover, we also studied the stability of the sensor. After the electrode was stored in a 4 °C refrigerator for 28 days, 92.6% of the original peak current was retained. Hence, the electrochemical biosensor was highly stable.

4. Conclusion

In summary, we successfully developed a highly sensitive and specific electrochemical biosensor to quantitatively detect multiple DNA methylation sites on the basis of the specificity to methylated cytosine after binding of GO with anti-5-methylcytosine antibody. Steric hindrance was utilized to further localize a single methylated site. Notably, the limit of detection was as low as 1 fM owing to GO signal amplification and HRP-IgG catalysis, which was significantly lower than those of most currently available methods. Furthermore, this method was simple, without requiring complicated processes such as bisulfite treatment and PCR amplification. The findings verify that this method is feasibly applicable to the early clinical diagnosis as well as risk evaluation of cancers and other related diseases.

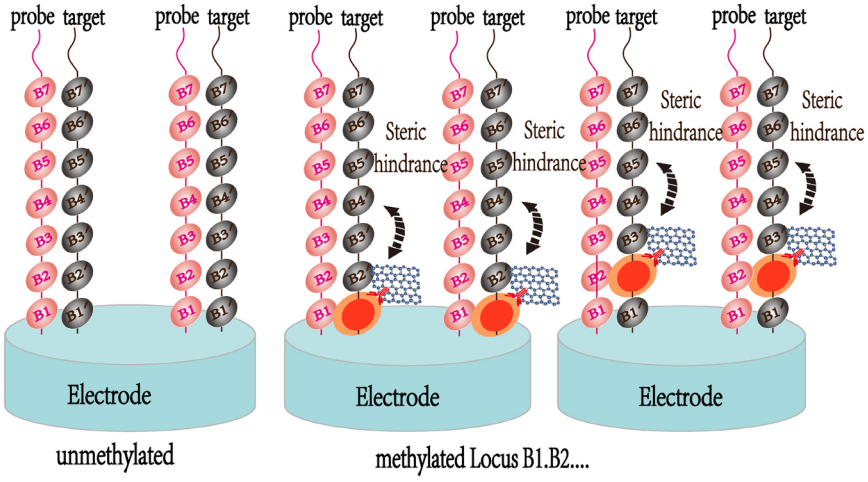

Fig. 6. Schematic representation of steric hindrance difference between hydrophobic methyl spheres and electrode surface after different methylated sites of target DNA sequences bind the probe. Left: Unmethylated double-stranded DNA that cannot bind antibody-modified GO; middle: binding of methylated cytosine which is closest to the electrode to antibody-modified GO, which generates steric hindrance; right: binding of methylated cytosine which is next closest to the electrode to antibody-modified GO, which induces steric hindrance differences.

CRediT authorship contribution statement

Jian Huang: Data curation, Writing - original draft. **Shu Zhang:** Data curation, Writing - original draft. **Fei Mo:** Conceptualization, Methodology. **Shasha Su:** Methodology, Software. **Xi Chen:** Data curation, Software. **Yan Li:** Supervision. **Lichao Fang:** Visualization. **Hui Huang:** Software, Validation. **Jun Deng:** Data curation, Software. **Huamin Liu:** Software, Validation. **Xiaoli Yang:** Writing - review & editing, Supervision. **Junsong Zheng:** Writing - review & editing, Supervision.

Acknowledgments

Financial support for this work was provided by the National Natural Science Foundation of China (Nos. 81572078, 81401722 and 81873982), the Third Military Medical University Medical Creative Research Foundation (SWH2016JCYB-62 and SWH2016JCYB-33).

Competing interests

The authors have declared that no competing interest exists.

Appendix A. Supplementary material

Supplementary data associated with this article can be found in the online version at doi:10.1016/j.bios.2018.12.022.

References

Agrawal, S., Unterberg, M., Koschmieder, S., zur Stadt, U., Brunnberg, U., Verbeek, W., Büchner, T., Berdel, W.E., Serve, H., Müller-Tidow, C., 2007. Cancer Res. 67, 1370–1377.
Andresen, K., Boberg, K.M., Vedeld, H.M., Honne, H., Jebsen, P., Hektoen, M., Wadsworth, C.A., Clausen, O.P., Lundin, K.E., Paulsen, V., et al., 2015. Hepatology 61, 1651–1659.
Assenov, Y., Müller, F., Lutsik, P., Walter, J., Lengauer, T., Bock, C., 2014. Nat. Methods 11, 1138–1140.
Bakshi, A., Ekram, M.B., Kim, J., 2015. Genom. Data 3, 87–89.
Bock, C., Halbritter, F., Carmona, F.J., Tierling, S., Datlinger, P., Assenov, Y., Berdasco, M., Bergmann, A.K., Booher, K., Busato, F., et al., 2016. Nat. Biotechnol. 34, 726–737.
Cheow, L.F., Quake, S.R., Burkholder, W.F., Messerschmidt, D.M., 2015. Nat. Protoc. 10, 619–631.
Coppedè, F., 2014. Cancer Lett. 342, 238–247.
Deng, X., Chen, M., Fu, Q., Smeets, N.M., Xu, F., Zhang, Z., Filipe, C.D., Hoare, T., 2016. ACS Appl. Mater. Interfaces 8, 1893–1902.
Flusberg, B.A., Webster, D.R., Lee, J.H., Travers, K.J., Olivares, E.C., Clark, T.A., Korlach, J., Turner, S.W., 2010. Nat. Methods 7, 461–465.
Gao, F., Fan, T., Ou, S., Wu, J., Zhang, X., Luo, J., Li, N., Yao, Y., Mou, Y., Liao, X., et al., 2017. Biosens. Bioelectron. 99, 201–208.
Gong, Y., Qin, C., He, W., Qiao, Z., Zhang, G., Chen, R., Gao, Y., Xiao, L., Jia, S., 2017. RSC Adv. 7, 53362–53372.
Guo, S., Diep, D., Plongthongkum, N., Fung, H.L., Zhang, K., Zhang, K., 2017. Nature 49, 635–642.
Hansen, K.D., Timp, W., Bravo, H.C., Sabunciyan, S., Langmead, B., McDonald, O.G., Wen, B., Wu, H., Liu, Y., Diep, D., et al., 2011. Nat. Genet. 43, 768–775.
Haque, A.J., Park, H., Sung, D., Jon, S., Choi, S.Y., Kim, K., 2012. Anal. Chem. 84, 1871–1878.
Jin, L., Yang, K., Yao, K., Zhang, S., Tao, H., Lee, S.T., Liu, Z., Peng, R., 2012. ACS Nano 6, 4864–4875.
Jing, X., Cao, X., Wang, L., Lan, T., Li, Y., Xie, G., 2014. Biosens. Bioelectron. 58, 40–47.
Jones, P.A., Issa, J.P.J., Baylin, S., 2016. Nat. Rev. Genet. 17, 630–641.
Kader, F., Ghai, M., 2015. Forensic Sci. Int. 249, 255–265.
Kato, D., Goto, K., Fujii, S., Takatsu, A., Hirono, S., Niwa, O., 2011. Anal. Chem. 83, 7595–7599.
Kong, R.M., Song, Z.L., Meng, H.M., Zhang, X.B., Shen, G.L., Yu, R.Q., 2014. Biosens. Bioelectron. 54, 442–447.
Krejcova, L., Richtera, L., Hynek, D., Labuda, J., Adam, V., 2017. Biosens. Bioelectron. 97, 384–399.
Kurita, R., Arai, K., Nakamoto, K., Kato, D., Niwa, O., 2012. Anal. Chem. 84, 1799–1803.
Labib, M., Sargent, E.H., Kelley, S.O., 2016. Chem. Rev. 116, 9001–9090.
Laird, P.W., 2010. Nat. Rev. Genet. 11, 191–203.
Li, W., Wu, P., Zhang, H., Cai, C., 2012. Anal. Chem. 84, 7583–7590.
Lin, D.J., Wu, J., Wang, M., Yan, F., Ju, H., 2012. Anal. Chem. 84, 3662–3668.
Mahshid, S.S., Camiré, S., Ricci, F., Vallée-Bélisle, A., 2015. J. Am. Chem. Soc. 137, 15596–15599.
Mahshid, S.S., Ricci, F., Kelley, S.O., Vallée-Bélisle, A., 2017. ACS Sens. 2, 718–723.
Moore, L.D., Le, T., Fan, G., 2012. Neuropsychopharmacology 38, 23–38.
Mulqueen, R.M., Pokholok, D., Norberg, S.J., Torkenczy, K.A., Fields, A.J., Sun, D., Sinnamon, J.R., Shendure, J., Trapnell, C., O'Roak, B.J., et al., 2018. Nat. Biotechnol. 36, 428–431.
Muren, N.B., Barton, J.K., 2013. J. Am. Chem. Soc. 135, 16632–16640.
Natarajan, A., Devi, K.S., Raja, S., Senthil Kumar, A., 2017. Sci. Rep. 7, 46169.
Saleem, W., Salinas, C., Watkins, B., Garvey, G., Sharma, A.C., Ghosh, R., 2016. Biosens. Bioelectron. 86, 522–529.
Schalkwyk, L.C., Meaburn, E.L., Smith, R., Dempster, E.L., Jeffries, A.R., Davies, M.N., Plomin, R., Mill, J., 2010. Am. J. Hum. Genet. 86, 196–212.
Schubeler, D., 2015. Nature 517, 321–326.
Smith, Z.D., Meissner, A., 2013. Nat. Rev. Genet. 14, 204–220.
Stefansson, O.A., Moran, S., Gomez, A., Sayols, S., Arribas-Jorba, C., Sandoval, J., Hilmarsdottir, H., Olafsdottir, E., Tryggvadottir, L., Jonasson, J.G., et al., 2015. Mol. Oncol. 9, 555–568.
Stieglitz, E., Mazor, T., Olshen, A.B., Geng, H., Gelston, L.C., Akutagawa, J., Lipka, D.B., Plass, C., Flotho, C., Chehab, F.F., et al., 2017. Nat. Commun. 8, 2127.
Tian, A.X., Yang, Y., Ying, J., Li, N., Lin, X.L., Zhang, J.W., Wang, X.L., 2014. Dalton Trans. 43, 8405–8413.
Visvanathan, K., Fackler, M.S., Zhang, Z., Lopez-Bujanda, Z.A., Jeter, S.C., Sokoll, L.J., Garrett-Mayer, E., Cope, L.M., Umbricht, C.B., Euhus, D.M., et al., 2016. J. Clin. Oncol. 35 (JCO2015662080).
Wan, Y., Wang, Y., Wu, J., Zhang, D., 2011. Anal. Chem. 83, 648–653.
Wang, M., Xu, Z., Chen, L., Yin, H., Ai, S., 2012. Anal. Chem. 84, 9072–9078.
Xu, C., Shi, X., Ji, A., Shi, L., Zhou, C., Cui, Y., 2015. PLoS One 10, e0144842.
Xu, R.H., Wei, W., Krawczyk, M., Wang, W., Luo, H., Flagg, K., Yi, S., Shi, W., Quan, Q., Li, K., et al., 2017. Nat. Mater. 16, 1155–1161.
Xu, Z., Yin, H., Huo, L., Zhou, Y., Ai, S., 2014. Sens. Actuators B Chem. 192, 143–149.
Yang, M., Javadi, A., Li, H., Gong, S., 2010. Biosens. Bioelectron. 26, 560–565.
Yang, Z., Wang, F., Wang, M., Yin, H., Ai, S., 2015. Biosens. Bioelectron. 66, 109–114.
Yao, G., Jie, W., Shao, L., Yan, F., Ju, H., 2014. Biosens. Bioelectron. 61, 593–597.
Yin, H., Sun, B., Zhou, Y., Wang, M., Xu, Z., Fu, Z., Ai, S., 2014. Biosens. Bioelectron. 51, 103–108.
Yu, J., Qin, B., Moyer, A.M., Nowsheen, S., Liu, T., Qin, S., Zhuang, Y., Liu, D., Lu, S.W., Kalari, K.R., et al., 2018. J. Clin. Investig. 128, 2376–2388.
Zhang, H., Guo, Z., Dong, H., Chen, H., Cai, C., 2017. Analyst 142, 2013–2019.
Zhang, L., Wei, M., Gao, C., Wei, W., Zhang, Y., Liu, S., 2015. Biosens. Bioelectron. 73, 188–194.
Ziller, M.J., Hansen, K.D., Meissner, A., Aryee, M.J., 2015. Nat. Methods 12, 230–232.